Molecular orbital polarization in $Na_2Ti_2Sb_2O$: Microscopic route to metal-metal transition without spontaneous symmetry breaking

Heung-Sik Kim[1] and Hae-Young Kee[1,2,*]

[1]*Department of Physics and Center for Quantum Materials, University of Toronto, 60 St. George St., Toronto, Ontario M5S 1A7, Canada*

[2]*Canadian Institute for Advanced Research / Quantum Materials Program, Toronto, Ontario MSG 1Z8, Canada*

(Received 17 August 2015; revised manuscript received 26 October 2015; published 10 December 2015)

Ordered phases such as charge- and spin-density wave state accompany either full or partial gapping of Fermi surface (FS) leading a metal-insulator or metal-metal transition (MMT). However, there are examples of MMT without any signatures of symmetry breaking. One example is $Na_2Ti_2Sb_2O$, where a partial gapping of FS is observed but a density wave ordering has not been found. Here we propose a microscopic mechanism of such a MMT, which occurs due to a momentum-dependent spin-orbit-coupled molecular orbital polarization. Since a molecular d orbital polarization is present due to a small spin-orbit coupling of Ti, there is no spontaneous symmetry breaking involved. However, a sharp increase of polarization happens above a critical electron interaction which gaps out the d orbtial FS and reduces the density of states significantly, while the rest of FS associated with Sb p orbtials is almost intact across MMT. Experimental implications to test our proposal and applications to other systems are also discussed.

DOI: 10.1103/PhysRevB.92.235121 PACS number(s): 71.20.Be, 71.70.Ej, 75.30.Gw, 75.70.Tj

I. INTRODUCTION

Fermi surface (FS) is one of most important concepts in solid state physics and exists in every metal, semimetal, and doped semiconductors. Many ordered phases, such as charge- and spin-density waves, and superconductivity can be regarded as FS instabilities. Such ordered phases accompany broken symmetries involving either translation, time-reversal, or charge conservation symmetries. As a consequence, either full or partial gapping of FS occurs with anomalies in spin susceptibility, specific heats, and resistivity at a critical temperature T_c [1].

However, there are examples of metallic systems that undergo a phase transition to a metallic state with a partial gapping of FS at lower temperatures without any detection of spontaneous symmetry breaking. A widely studied example is URu_2Si_2, where both f and d orbitals are relevant and a low-temperature metallic phase is associated with a hidden order, implying difficulties of identifying the order parameter [2,3]. A less-studied material is $Na_2Ti_2Sb_2O$ (NTSO), where Ti d orbitals and Sb p orbtials play a major role in determining physical properties [4,5]. NTSO shows a metal-metal transition (MMT) around $T_c \simeq 115$ K, where the temperature dependence of the resistivity above and below T_c indicates its metallic behavior, while the increase of resistivity and reduction of susceptibility at T_c imply the reduction of density of states (DOS) at the Fermi level [6–8]. An angle-resolved photoemission measurement observed partial gapping of the Fermi surface below T_c [9], and specific heat versus T shows a sharp peak at T_c, signifying substantial entropy change [10]. Previous studies have proposed possible charge- and spin-density wave instabilities for the origin of MMT [11–13]; however, there is no experimental evidence of charge- and spin-density wave order. ^{23}Na nuclear magnetic resonance measurement revealed no sign of enhanced spin fluctuations or magnetic order [14], and neutron and x-ray diffraction data found only changes in lattice constants across T_c [6,15].

In this work, we provide a microscopic route to MMT without spontaneous symmetry breaking in NTSO [16]. Figure 1 illustrates our proposal; a momentum-dependent polarization of molecular orbitals (MO), which is induced by the cooperation of spin-orbit coupling (SOC) and the onsite Coulomb interaction inherent in Ti $3d$ orbital, gaps out a significant fraction of FS while leaving the rest of FS intact, so that the system remains metallic. As shown in Fig. 1(a), the system has three Fermi surfaces with atomic Sb p, Ti d, and MO originating from Ti d orbitals at Γ, X, and M points in the Brillouin zone, respectively. Degeneracies at Γ and M points are protected by crystal and SU(2) spin rotational symmetries, thus introduction of SOC of Sb p and Ti d lifts degeneracies at Γ and M, respectively. Due to the smallness of Ti SOC, it makes a tiny gap at M point and the MO states evolve into spin-orbit coupled MO (SO-MO) states as shown in Fig. 1(b). Inclusion of the Coulomb interaction sharply enhances the SO-MO polarization, such that a significant gap opens at M point, reducing the FS area in Γ and X points to balance the charge as shown in Fig. 1(c). Neither lattice nor time-reversal symmetry (TRS) are broken in the resulting metallic state. Due to the lack of spontaneously broken symmetry MMT is a first-order phase transition, which we will discuss later. The spin-orbit coupled and anisotropic nature of the SO-MO states can explain the strong anisotropies in electronic and magnetic responses observed in recent experiments [10,15]. While our theory is applied to NTSO, it can be generalized to a system with different orbital characters that compose FS and undergoes a partial gapping of FS across MMT.

II. STRUCTURE AND *AB INITIO* CALCULATIONS

Crystal structure of NTSO consists of neighboring Ti_2Sb_2O layers with Na ions intercalated in between. As shown in Fig. 2(a), each Ti_2Sb_2O layer is composed of a Ti_2O square lattice and two $TiSb_2$ ribbons perpendicular to each other, with

*hykee@physics.utoronto.ca

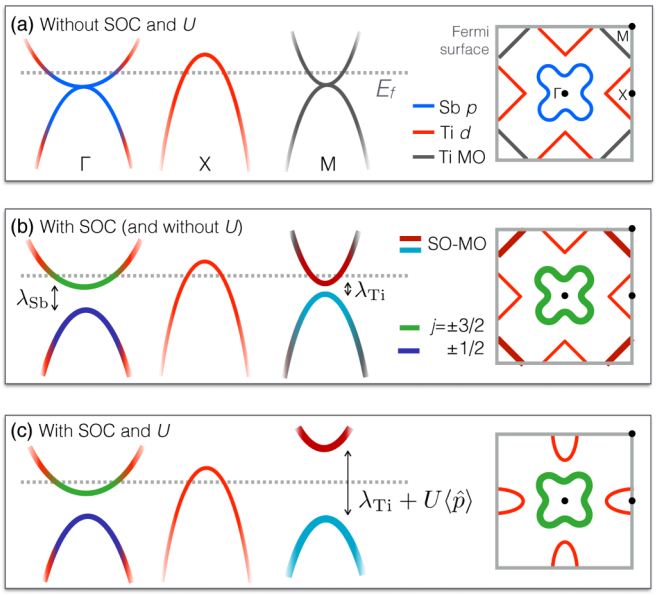

FIG. 1. (Color online) Schematic figures illustrating evolution of electronic structures in NTSO upon inclusion of spin-orbit coupling (SOC) and on-site Coulomb interaction U. Panels (a) and (b) show schematic band structures near three special k points and Fermi surfaces without and with the presence of SOC. As depicted in panel (c), the Coulomb interaction enhances the polarization ($\langle\hat{p}\rangle$) of the spin-orbit coupled molecular orbital (SO-MO) states near M point. Line colors depict the orbital character as shown in the figure, and thicker lines represent the states affected by inclusion of SOC.

the unit cell containing two Ti sites in a NTSO layer (Ti1 and Ti2 shown in Fig. 2). The space group for the whole unit cell, which contains two NTSO layer, is $I4/mmm$ (No. 139), and for an isolated NTSO layer the layer group is $P4/mmm$ (No. 123).

Previous *ab initio* studies showed that strong hybridization between the Ti d and Sb p orbitals yields dispersive bands for both states so that the system has multiple Fermi surfaces with d and p orbital character as shown in Fig. 1 [11,12]. Contrary to the p orbital pocket at Γ, which shows three-dimensional shape, the d orbital pockets show weak dispersion along the layer-normal direction and considered as quasi-two-dimensional Fermi surfaces. While we simplify the system by choosing an isolated NTSO layer as a unit cell, comparison between the band structures from the full and our two-dimensional unit cells in Appendix B [17] shows almost unaffected d bands near the zone boundary by the layer stacking. In order to understand the combined effects of SOC and electronic correlations on FS reduction without symmetry breaking, magnetism is not considered in this study. However, we note that our paramagnetic solution is higher in energy than the magnetic solutions discussed in the previous studies [12,13]. To enforce paramagnetic solutions all calculations are initially started without any magnetic configuration.

Figure 2(a) shows the Ti d orbitals which contribute to the bands near the Fermi level: $\{|d_{xy}\rangle_1, |d_{e_g}\rangle_1\}$ and $\{|d_{xy}\rangle_2, |d_{e_g}\rangle_2\}$ for Ti1 and Ti2, respectively, where the subscripts 1 and 2 denote the Ti atoms to which the orbitals belong. The hybrid $|d_{e_g}\rangle_{1,2}$ orbitals are defined as linear combinations of

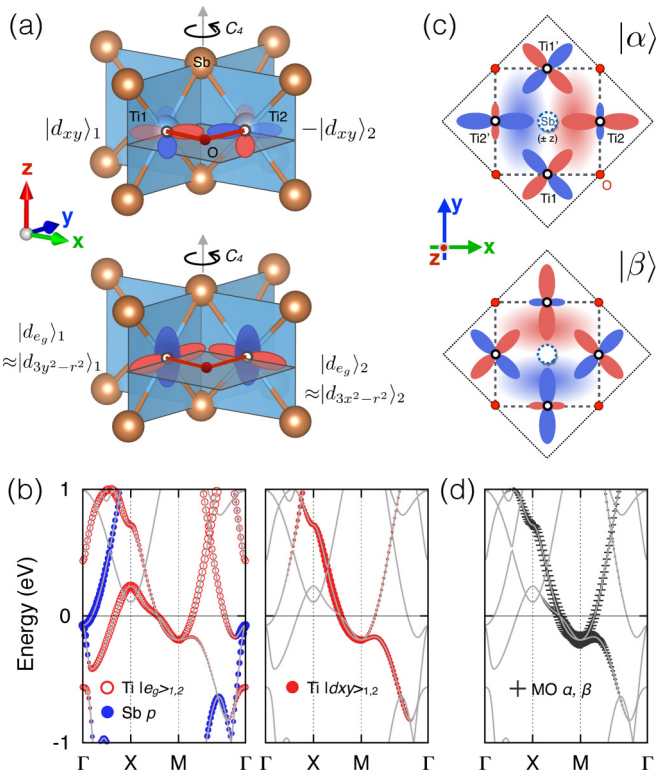

FIG. 2. (Color online) (a) Crystal structure of single Ti_2Sb_2O layer with dominant Ti d orbitals near the Fermi level—$\{|d_{xy}\rangle_1, |d_{e_g}\rangle_1\}$ and $\{|d_{xy}\rangle_2, |d_{e_g}\rangle_2\}$ for Ti1 and 2, respectively—depicted in the figure. Note that Ti1 and Ti2 sites are transformed to each other by the C_4 rotation along the $\hat{z}$ axis. (b) Band structure of single layer NTSO without including SOC and Coulomb interaction. Left panel shows orbital weights of Sb p and Ti $|d_{e_g}\rangle_{1,2}$ within the Bloch states with the weight proportional to the size of corresponding symbols. Right panel shows Ti $|d_{xy}\rangle_{1,2}$ orbital weights. (c) Schematic figures of two degenerate α and β states at M point depicted in the $\sqrt{2} \times \sqrt{2}$ times enlarged unit cell (original and enlarged unit cells represented as dashed and dotted square, respectively) as MOs. Bands with the weights of the α and β MO states are shown in panel (d).

e_g orbitals such that $|d_{e_g}\rangle_1 \equiv -a|d_{x^2-y^2}\rangle_1 - b|d_{3z^2-r^2}\rangle_1$ and $|d_{e_g}\rangle_2 \equiv +a|d_{x^2-y^2}\rangle_2 - b|d_{3z^2-r^2}\rangle_2$, where the real coefficients a and b are determined by the ligand fields. Note that $|d_{e_g}\rangle_{1,2}$ are dominated by $|d_{3y^2-r^2}\rangle_1$ and $|d_{3x^2-r^2}\rangle_2$, respectively, in our system, and $|d_{xy}\rangle_1$ and $|d_{e_g}\rangle_1$ are transformed to $-|d_{xy}\rangle_2$ and $|d_{e_g}\rangle_2$, respectively, by the C_4 rotation depicted in the figure. Left panel of Fig. 2(b) shows the bands without SOC where the orbital weights of Sb p and $|d_{e_g}\rangle_{1,2}$ states are represented as the size of the corresponding symbols. The $|d_{xy}\rangle_{1,2}$ weight is concentrated on the X-M line as shown in the right panel in the figure.

Both the Γ and M points have D_{4h} point group symmetry, which allows the presence of quadratic band touching points located just below the Fermi level, as can be seen in Fig. 2(b). At Γ point, the band touching consists of Sb atomic p_x and p_y orbitals where degeneracy of the orbitals is compatible with the Sb site symmtery (C_{4v}). On the contrary, the band touching at M point has dominant d character and described by molecular orbitals (MO). Without considering spin, two degenerate Bloch states at M point, which we denote as $|\alpha\rangle$

and $|\beta\rangle$, are expressed as follows:

$$|\alpha\rangle \approx \sum_{\mathbf{R}} e^{i\mathbf{k}_M\cdot\mathbf{R}}(|d_{xy}\rangle_{\mathbf{R},1} + |d_{e_g}\rangle_{\mathbf{R},2}),$$

$$|\beta\rangle \approx \sum_{\mathbf{R}} e^{i\mathbf{k}_M\cdot\mathbf{R}}(-|d_{e_g}\rangle_{\mathbf{R},1} - |d_{xy}\rangle_{\mathbf{R},2}),$$

where $\mathbf{k}_M = (\frac{\pi}{a}, \frac{\pi}{a})$, $\mathbf{R}$, and $\{1,2\}$ are indices for Bravais lattice and Ti sublattices, respectively. Figure 2(c) shows the schematic illustrations of the states, where the dashed and dotted squares depict the primitive and the enlarged unit cell. Like the Sb p_x and p_y orbitals at Γ point, they belong to the E_u irreducible representation, which are odd under spatial inversion and transforms as $(C_4)^2|\alpha\rangle = C_4|\beta\rangle = -|\alpha\rangle$. There is additional degeneracy due to the SU(2) symmetry in the spin subspace without the presence of SOC, so the band touching at M point is fourfold degenerate and protected by the SU(2) and crystal symmetries. Unless either the spin or the crystal symmetry is lifted, the degeneracy at M point remains robust, and our LDA+U calculation without including SOC and keeping paramagnetic constraint confirms it (See Apendix E).

III. DEGENERACY LIFTING AT Γ AND M POINTS VIA SOC

Below we discuss the effect of SOC. Intuitively, one expects a relatively large impact of SOC on Sb p orbitals while negligible on Ti d orbtials, as SOC in Ti is only about 20 meV. Indeed, degenerate bands near Γ point made of p orbitals are split, and the gap between the two is about 0.4 eV. Each band is characterized by total angular momenta $j = 1/2$ and $3/2$ made of $|l_z = \pm 1\rangle = |p_x \pm ip_y\rangle$ and spin-1/2 due to ligand field spitting of layer structure. As SOC is introduced, the SU(2) symmetry in the spin space is lifted, and the fourfold degeneracy at Γ is split into $j = 1/2$ and $3/2$ doublets as shown in Fig. 3(a). Hereafter we denote the orbital and total angular momenta for the atomic and MO states as lowercase and capital letters, respectively.

Similarly, at M point, quenching of planar orbital moment components happens in the MO space $\{|\alpha\rangle, |\beta\rangle\}$. Projecting the Ti total angular momentum operators $\hat{\boldsymbol{L}} \equiv \hat{\boldsymbol{l}}^{\mathrm{Ti1}} \oplus \hat{\boldsymbol{l}}^{\mathrm{Ti1}'} \oplus \hat{\boldsymbol{l}}^{\mathrm{Ti2}} \oplus \hat{\boldsymbol{l}}^{\mathrm{Ti2}'}$ onto the space yields $\hat{L}_z$ as the only nonvanishing component, which is diagonalized with the basis choice of $|L_z^{\pm}\rangle \equiv |\alpha \mp i\beta\rangle$, where $L_z^{\pm} \approx \pm\sqrt{3}$ in this system [18]. In the presence of Ti SOC, the $|L_z^{\pm}\rangle$ states are split into two spin-orbit-coupled MO (SO-MO) doublets, which are characterized by total angular momenta $J = (|L_z^{\pm}| + \frac{1}{2}) \equiv J^+$ and $(|L_z^{\pm}| - \frac{1}{2}) \equiv J^-$. Note that both J^+ and J^- form doublets with $J_z^+ = \pm(|L_z^{\pm}| + \frac{1}{2})$ and $J_z^- = \pm(|L_z^{\pm}| - \frac{1}{2})$, respectively, and J^+ doublet is higher in energy than J^- by 20 meV at M point as shown in the inset of Fig. 3(a).

IV. MOLECULAR ORBITAL POLARIZATION ENHANCED BY ONSITE COULOMB INTERACTION

The size of the gap opening can be quantified by defining the MO polarization operator $\hat{p} \equiv \hat{n}_{J^-} - \hat{n}_{J^+}$, where $\hat{n}_{J^\pm}$ are number operators for the $J^\pm$ subspaces. SOC in the MO space can be rewritten by employing the MO polarization operator as

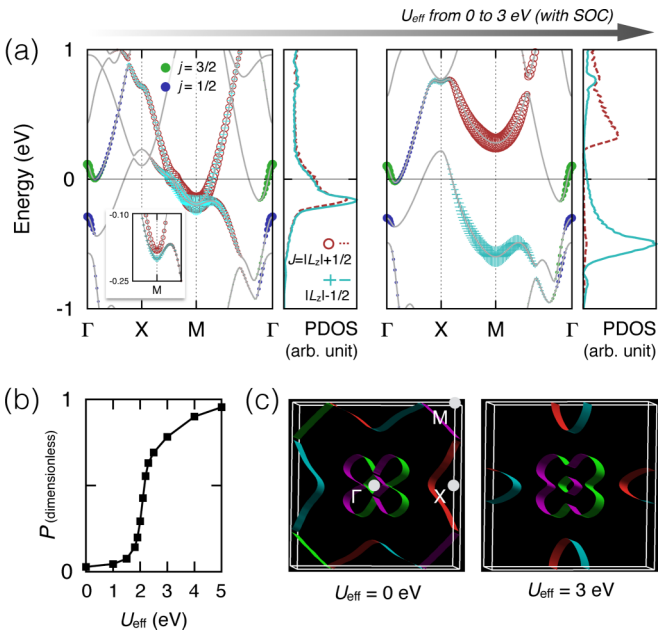

FIG. 3. (Color online) (a) Band structures and PDOS projected onto the SO-MO states without (left panel) and with including the onsite Coulomb interaction ($U_{\mathrm{eff}} = 3$ eV, right panel) in the presence of SOC. Orbital weights of Sb $j = 3/2$, $1/2$, and SO-MO states are depicted as the size of the symbols indicating each state. Magnified view of bands near M point is shown in the inset. (b) A plot of normalized MO polarization P between the SO-MO states as a function of U_{eff}. (c) Fermi surfaces of systems without (left panel) and with the Coulomb interactions (right panel).

$\hat{H}_{\mathrm{SO}} = -\lambda_{\mathrm{Ti}}\hat{p}/2$. Due to the minus sign, $\hat{H}_{\mathrm{SO}}$ favors positive MO polarization, but its magnitude is tiny because of the small $\lambda_{\mathrm{Ti}} \sim 20$ meV as can be seen in the projected density of states (PDOS) of Fig. 3(a). However, once the degeneracy at M is lifted, the size of the splitting can be further enhanced, and inclusion of onsite Coulomb interaction does the role in this case.

Like $\hat{H}_{\mathrm{SO}}$, the LDA+U correction to the Ti onsite potential introduced by the Coulomb interaction can be projected onto the MO space. It can be rewritten in terms of $\hat{p}$ as follows [19]:

$$\hat{V}_U \equiv U_{\mathrm{eff}}\left[\left(\frac{1}{2} - \frac{\langle\hat{n}\rangle}{4}\right)\hat{n} - \frac{\langle\hat{p}\rangle}{2}\hat{p}\right],$$

where $U_{\mathrm{eff}} \equiv U - J$ is the effective Coulomb interaction parameter, $\hat{n} \equiv \hat{n}_{J^+} + \hat{n}_{J^-}$ is the total number operator, and expectation values are obtained by integrating over the Brillouin zone (detailed derivation is in Appendix C). Combining it with $\hat{H}_{\mathrm{SO}}$, apart from the trivial constant term, yields

$$\hat{H}_{\mathrm{SO}} + \hat{V}_U = -\frac{\lambda_{\mathrm{Ti}} + U_{\mathrm{eff}}\langle\hat{p}\rangle}{2}\hat{p},$$

so that the MO polarization $\langle\hat{p}\rangle$ initiated by SOC can be further increased under the presence of U_{eff}. Right panel in Fig. 3(a) shows the band structure and PDOS projected onto the SO-MO states with the presence of $U_{\mathrm{eff}} = 3$ eV. The gap at M point is allowed due to the loss of SU(2) symmetry via SOC, and is greatly enhanced by the inclusion of the Coulomb interaction. A normalized MO polarization $P \equiv \langle\hat{p}\rangle/\langle\hat{n}\rangle$ as a

function of U_{eff} is plotted in Fig. 3(b). One can see an abrupt change in P near $U_{\text{eff}}^{c} = 2.2$ eV, where the bottom of the $(|L_z^{\pm}| + \frac{1}{2})$ band crosses the Fermi level and the electron-like Fermi pocket near M point disappears. Figure 3(c) compares the Fermi surfaces with and without including $U_{\text{eff}} = 3$ eV. To compensate the removal of the M point electron pocket, the size of hole-like pocket near X point also decreases, resulting in the half-reduction of the Fermi surface area. Such reduction of Fermi surface area, or equivalently the reduction of DOS at the Fermi level, is observed in several magnetic susceptibility and resistivity measurements [6,7,10].

We also comment on the X pocket, which is less affected by the inclusion of U_{eff} than the M pocket despite its dominant $|d_{e_g}\rangle_{1,2}$ character. Since the X pocket coexists with the p-originated Γ pocket, the size of X pocket is determined by the onsite energy of $|d_{e_g}\rangle_{1,2}$ orbitals relative to that of Sb p. The $\hat{V}_U$ term, however, behaves as an effective SOC for the SO-MO states, and its contribution to the $|d_{e_g}\rangle_{1,2}$ onsite energy is not significant, so that the X pocket remains even after inclusion of the Coulomb interaction. This is confirmed by examining the change of the onsite energies from the Wannier orbital calculations for the Ti d states. Note also that the Sb $j = 3/2$ and $1/2$ states near Γ are well polarized due to the large λ_{Sb}, so they are less affected by the inclusion of U_{eff}.

V. DISCUSSION AND CONCLUSION

The notion of orbital polarization in transition metal compounds, which is induced by the Coulomb interaction in degenerate d orbitals, usually accompanies symmetry lowering by the orbital-lattice coupling such as Jahn-Teller effect [20–25]. In metallic systems, an orbital polarization also occurs [26], but does not accompany a MMT for a fixed charge filling. The SO-MO polarization in our work is distinguished from previous studies since it does not accompany a spontaneous symmetry reduction.

For experimental validation of our proposal, one can take advantage of the anisotropy in the SO-MO states. Since the total angular momentum of the SO-MO states are fixed to be perpendicular to the Ti_2O plane, i.e., the absence of the in-plane angular momentum component, one direct consequence of the SO-MO formation is an anisotropic response to the external magnetic fields. A recent report on the magnetic susceptibility of NTSO shows such anisotropic behavior, where the $H//z$ susceptibility data shows drastic enhancement compared to the $H//xy$ result below the transition temperature [10]. Such behavior is hard to understand in the conventional charge-density wave picture but is consistent with our SO-MO polarization scenario; due to the absence of the $\hat{L}_{x,y}$ components in the SO-MO space, the states should be more susceptible to $H//z$ compared to the in-plane fields.

Measuring the branching ratio in Ti L_2 and L_3 edge x-ray absorption spectroscopy (XAS) below T_c can be another way to experimentally validate the MO polarization scenario [27]. Note that the unoccupied SO-MO state has total angular momentum of $j^{+} = (|l_z^{\pm}| + \frac{1}{2})$, which is close to $5/2$, for each Ti site. As a result, L_3 edge XAS is expected to show higher intensity more than twice that of L_2 edge, so that the ratio between the L_3 and L_2 channels should be larger then the statistical ratio 2:1. Also, phase-sensitive tools such as resonant x-ray scattering may probe the presence of SO-MO states, which revealed the presence of the spin-orbit-entangled $j_{\text{eff}} = 1/2$ states in several iridate compounds with strong SOC [28,29].

Finally, we would like to mention the nature of the phase transition at T_c. Specific heat versus temperature data indicate significant loss of entropy at the transition. Previously this was considered as a signature of continuous phase transition by the density wave formation, but this feature can be explained within our SO-MO polarization scenario, which results in entropy change by the reduction of the Fermi surface area. Since this process does not spontaneously break any symmetries in NTSO, it should be a first-order transition. We found a metastable phase with $P \sim 0$ in the regime $2.3 \leqslant U_{\text{eff}} \leqslant 4$ eV and its presence is robust independent of parameters and code choices (see Appendix D for details on the metastable state). Remarkably, hysteresis behavior in resistivity with unknown origin was reported previously [7], indicating a possible first-order phase transition.

In summary, we propose an alternative scenario for the MMT in NTSO based on the SO-MO polarization induced by SOC and the Coulomb interaction. Our picture can be generalized to other systems with FS with mixed orbital characters and spontaneous phase transition with partial gapping out of FS without a symmetry breaking. Also, our picture calls attention to the role of SOC in $3d$ transition metal compounds, which was considered insignificant in understanding the physics of such systems. Indeed, there are several reports about the role of the ostensibly small SOC, which cooperate with the Coulomb interaction and becomes a crucial element for the underlying physics [30–32]. Further studies on the role of SOC in previously known transition metal systems with high crystal symmetries can be an interesting future subject in this regard.

ACKNOWLEDGMENTS

H.Y.K. thanks the Kavli Institute for Theoretical Physics at Santa Barbara for hospitality. This work was supported by the NSERC of Canada and the center for Quantum Materials at the University of Toronto. Computations were mainly performed on the GPC supercomputer at the SciNet HPC Consortium. SciNet is funded by: the Canada Foundation for Innovation under the auspices of Compute Canada; the Government of Ontario; Ontario Research Fund-Research Excellence; and the University of Toronto.

APPENDIX A: COMPUTATIONAL DETAILS

For the electronic structure calculations with SOC and onsite Coulomb interaction, OPENMX code [33,34], which is based on the linear-combinaion-of-pseudo-atomic-orbital basis formalism, was used. A noncollinear DFT scheme and a fully relativistic j-dependent pseudopotential were used to treat SOC, and the parametrization of Perdew and Zunger for the local density approximation was chosen for the exchange-correlation functional [37,38]. 400 Ry of energy cutoff and $16\times16\times1$ of k grid were used for the real-space and momentum-space integrations, respectively. Onsite Coulomb interaction was treated via a rotationally invariant DFT+U

formalism implemented in OPENMX code [39,40], and up to 5.0 eV of $U_{\rm eff} \equiv U - J$ parameter were used for Ti d orbital in our DFT+SOC+U calculations.

For a double-checking purpose of OPENMX results and optimization of the lattice with the presence of SOC and $U_{\rm eff}$, Vienna *ab initio* simulation package (VASP) [35,36] code was employed in which projector-augmented wave potentials are implemented. 500 eV of plane-wave energy cutoff for the basis set and PBEsol [41] exchange-correlation functional were used for the calculations. The force criterion was 10^{-3} eV/Å. Changes of internal coordinates due to the inclusion of $U_{\rm eff}$ were negligible. Note that in our calculations we did not consider magnetic ordering.

APPENDIX B: COMPARISON BETWEEN SINGLE-LAYER AND FULL UNIT CELL RESULTS

Figure 4(a) compares the single-layered unit cell that we employed in this work to the full unit cell of $Na_2Ti_2Sb_2O$ (NTSO). Due to the layered structure with weak coupling between adjacent layers, the electronic structure shows a quasi-two-dimensional character as shown in Fig. 4(b), which shows the band structures and PDOS for Ti and Sb atoms without the presence of SOC and the Coulomb interaction. Solid and dashed lines represent bands from the single-layered and the full unit cell, respectively. As mentioned above, only the Sb p bands near Γ point are affected by the layer stacking while Ti d and molecular orbital bands near the zone boundary are less affected. Especially, the Ti MO bands near M point in the single-layer calculation shows almost no difference compared to those from the full unit cell calculation, which justifies the choice of the two-dimensional unit cell in our work.

APPENDIX C: LDA+U CORRECTION IN TERMS OF MO POLARIZATION

Here we recast the LDA+U correction term $\hat{V}_U$ in our *ab initio* calculations in terms of the MO polarization operator $\hat{p}$. The derivation is based on the Dudarev's rotationally invariant LDA+U functional [39], which was implemented both in OPENMX [40] and VASP and was employed in this work. Note that, similar derivation was done with more general form of onsite Coulomb interaction previously [19].

The onsite Coulomb interaction contributes to the LDA+U total energy as follows [39,40]:

$$E_{\rm LDA+U} = E_{\rm LDA} + E_U^0 - E_{\rm dc}^U, \tag{C1}$$

where the onsite Coulomb interaction E_U^0 and the double counting term $E_{\rm dc}^U$ are

$$E_U^0 = \frac{1}{2}\sum_\alpha U_\alpha \sum_{\sigma m m'} n_{\alpha m}^\sigma n_{\alpha m'}^{-\sigma} + \sum_{\alpha, m\neq m'} n_{\alpha m}^\sigma n_{\alpha m'}^\sigma, \tag{C2}$$

$$E_{\rm dc}^U = \frac{1}{2}\sum_\alpha U_\alpha N_\alpha (N_\alpha - 1) - \frac{1}{2}\sum_\alpha J_\alpha \sum_\sigma N_\alpha^\sigma \left(N_\alpha^\sigma - 1\right), \tag{C3}$$

where α is a site-orbital shell (s, p, d, $\cdots$) compound index, and $\{m,m'\}$ and σ are indices for orbitals within each α shell and spin, respectively. $N_\alpha = \sum_\sigma N_\alpha^\sigma = \sum_{\sigma m} n_{\alpha m}^\sigma$ is the total occupation number for an α shell. It is straightforward to see that the energy correction to the LDA total energy $E_U \equiv E_U^0 - E_{\rm dc}^U$ can be expressed in terms of the density matrix of α shells as follows:

$$E_U = \frac{1}{2}\sum_\alpha U_{{\rm eff},\alpha}\{{\rm Tr}(n_\alpha) - {\rm Tr}(n_\alpha n_\alpha)\}, \tag{C4}$$

where $U_{{\rm eff},\alpha} \equiv U_\alpha - J_\alpha$ and the traces are done over the spin and orbital indices. Note that Eq. (C4) is invariant up to an unitary transform within each α shell, so that the density matrices can be diagonalized by choosing any convenient basis set. Hereafter we will choose such basis set with denoting the spin-orbit coupled (and site) index as μ. Taking derivative of Eq. (C4) with respect to the LCAO coefficients for μ orbitals yields an effective onsite potential $\hat{V}_U$ originating from the Coulomb interaction,

$$\hat{V}_U \equiv \sum_\mu U_{{\rm eff},\mu}\left(\frac{1}{2} - n_\mu\right)\hat{P}_\mu, \tag{C5}$$

where $\hat{P}_\mu$ is a projection operator to the μ orbital.

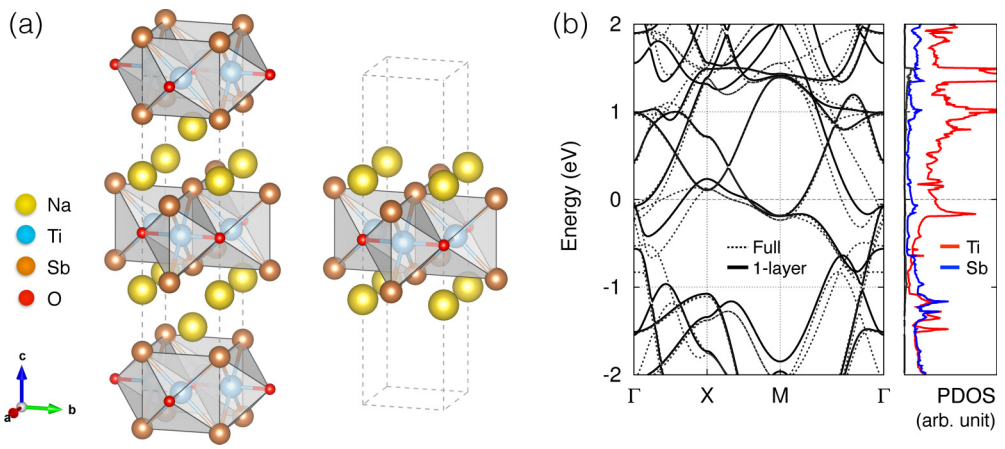

FIG. 4. (Color online) (a) Comparison of the full unit cell (left) and the single-layer unit cell (right), which adopted for the calculation. (b) Band structures and PDOS for Ti and Sb atoms without the presence of SOC and $U_{\rm eff}$. Solid and dashed lines in the band plot represent results from the single-layer and the full unit cell, respectively. PDOS is from the full unit cell calculation.

The spin-orbit-coupled MO (SO-MO) states can be expressed in terms of the local Ti orbital angular momentum eigenstates in the $\sqrt{2}\times\sqrt{2}$ times enlarged unit cell as follows:

$$\left|J_z=\pm\left(|L_z^{\pm}|+\frac{1}{2}\right)\right\rangle=\frac{1}{2}\sum_{a=1}^{4}(\pm i)^a|l_z^{\pm}\rangle_a\otimes|\uparrow\downarrow\rangle$$
$$\equiv\frac{1}{2}\sum_{a=1}^{4}(\pm i)^a\left|j_z=\pm\left(|l_z^{\pm}|+\frac{1}{2}\right)\right\rangle_a, \tag{C6}$$

$$\left|J_z=\pm\left(|L_z^{\pm}|-\frac{1}{2}\right)\right\rangle=\frac{1}{2}\sum_{a=1}^{4}(\pm i)^a|l_z^{\pm}\rangle_a\otimes|\downarrow\uparrow\rangle$$
$$\equiv\frac{1}{2}\sum_{a=1}^{4}(\pm i)^a\left|j_z=\pm\left(|l_z^{\pm}|=\frac{1}{2}\right)\right\rangle_a, \tag{C7}$$

where a is Ti site index (Ti1′ and 2′ in Fig. 2(c) in the main text correspond to $a=3$ and 4, respectively), and $|l_z^{\pm}\rangle_a$ are orbital angular momentum eigenstates for Ti site a with $l_z^{\pm}\simeq\pm\sqrt{3}$. Note that all of the constituent local Ti states within a SO-MO state are same except the phase factor. $\hat{V}_U$ is projected onto the SO-MO states and yields

$$\hat{V}_U^{\mathrm{MO}}\equiv U_{\mathrm{eff}}\sum_{\bar{\mu}}\left(\frac{1}{2}-n_{\bar{\mu}}\right)\hat{P}_{\bar{\mu}}, \tag{C8}$$

where $\bar{\mu}$ is now the SO-MO index and $n_{\bar{\mu}}$ is the occupation number for the SO-MO states.

From the results in the main text, we know that the SO-MO states are split into the $J^+\equiv(|L_z^{\pm}|+\frac{1}{2})$ and $J^-\equiv(|L_z^{\pm}|-\frac{1}{2})$ states. So we recast the SO-MO occupation numbers in terms of the average occupation and polarization as $n_{\bar{\mu}\in J^{\pm}}=\bar{n}\mp\frac{p}{2}$, projection operators in terms of the total occupation number operator $\hat{n}\equiv\sum_{\bar{\mu}}\hat{P}_{\bar{\mu}}$, and the orbital polarization operator $\hat{p}\equiv\hat{n}_{J^-}-\hat{n}_{J^+}=\sum_{\bar{\mu}\in J^-}\hat{P}_{\bar{\mu}}-\sum_{\bar{\mu}\in J^+}\hat{P}_{\bar{\mu}}$. Finally, we obtain

$$\hat{V}_U^{\mathrm{MO}}\equiv U_{\mathrm{eff}}\left[\left(\frac{1}{2}-\frac{n}{4}\right)\hat{n}-\frac{p}{2}\hat{p}\right], \tag{C9}$$

where $n=\langle\hat{n}\rangle$ and $p=\langle\hat{p}\rangle$.

APPENDIX D: METASTABLE PHASES WITH $P<0$ AND $P\sim0$

In the main text we presented the phase with MO polarization $P=P_+>0$. Two other minima with $P=P_0\sim0$ and $P=P_-<0$ are also found above $U_{\mathrm{eff}}\simeq2.3$ eV, and P_+ becomes a lowest energy solution above $U_{\mathrm{eff}}\simeq2.3$ eV. Figure 5(a) shows a plot of P for the $P_\pm$ and P_0 phases from the OPENMX calculations as a function of U_{eff}, where the band and PDOS of the P_- (left panel) and P_0 (right panel) phases at $U_{\mathrm{eff}}=2.5$ eV are shown in Fig. 5(b). Note that three minima are found in the region $2.3\lesssim U_{\mathrm{eff}}\lesssim4$ eV, which is marked by the vertical dashed lines in Fig. 5(a). In this metastable region, the energy difference between the P_+ and P_- is tiny (P_+ phase is slightly lower in energy by ~10 meV) and $|P_+|\simeq|P_-|$, while the P_0 phase is higher in energy than the other ones as shown in Fig. 5(c).

Presence of the P_0 phase is robust against choice of parameters and codes. Figure 5(c) shows total energy differences versus U_{eff} between the P_+ and P_0 phases from calculations with two different code and exchange-correlation functionals; dark cyan and yellow symbols depicting results from OPENMX and VASP codes, respectively. Contrary to OPENMX results, in VASP calculations full optimizations of lattice parameters and internal coordinates were performed for a better estimation of total energies. Note that, compared to OPENMX results, the energy differences are reduced with the metastable region slightly shifted to higher U_{eff} regime in VASP results.

Ignoring a small linear term (and odd powers) in P due to the small SOC of Ti, the three minima with $P_\pm$ and P_0 can be captured by a Ginzburg-Landau free energy $F(P)$ with a negative quartic term such as

$$F(P)\propto aP^2-bP^4+cP^6,\ (a,b,c>0). \tag{D1}$$

This shows three local minima at $P_0=0$ and $P_\pm=\pm\sqrt{\frac{b+\sqrt{b^2-3ac}}{3c}}$ when $b^2>3ac$, and it exhibits $P_\pm$ as global minima when $b^2\gtrsim9ac/2$ showing the first-order transition behavior.

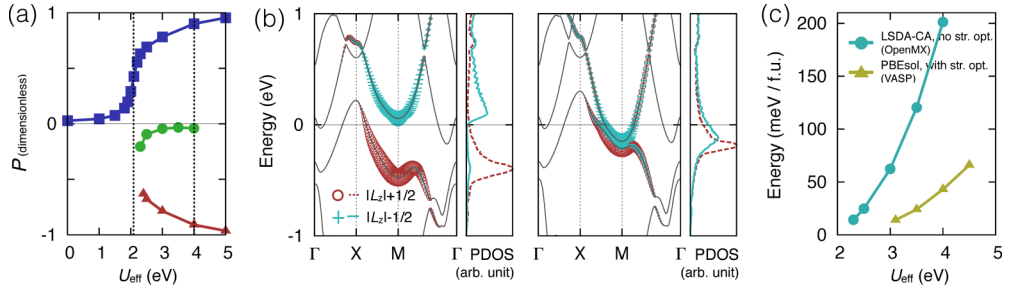

FIG. 5. (Color online) (a) P versus U_{eff} plot including the results from metastable states, where the results with $P_+>0$, $P_-<0$, and $P_0\sim0$ are depicted in blue, green, and red symbols, respectively. Vertical dashed lines mark the region $2.3\lesssim U_{\mathrm{eff}}\lesssim4$ eV that the P_0 phase remain stable (the P_+ phase is stabilized beyond $U_{\mathrm{eff}}=2.4$ eV). (b) SO-MO-projected bands and PDOS of metastable P_- (left panel) and P_0 (right panel) phases at $U_{\mathrm{eff}}=2.5$ eV. (c) Energy difference (per formula unit) vs. U_{eff} between the $P>0$ and $P\sim0$ phases. Dark cyan and yellow symbols represents result from OPENMX (with LSDA-CA functional, no structural optimization) and VASP (with PBEsol functional and lattice optimization), respectively.

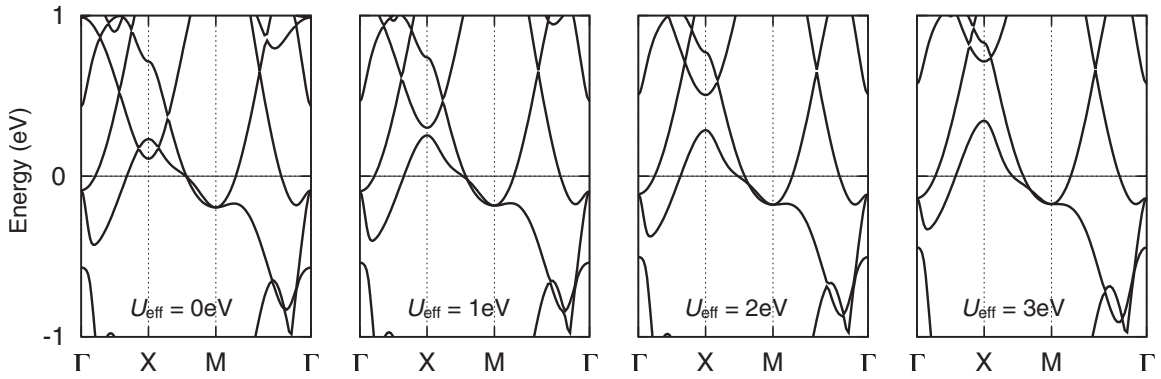

FIG. 6. Band structures from LDA+U calculations without including SOC. From left to right panels, bands with $U_{\text{eff}} = 0$, 1, 2, and 3 eV are shown.

APPENDIX E: LDA+U CALCULATIONS WITHOUT SOC

Figure 6 shows the band structures from LDA+U calculations without including SOC. Up to $U_{\text{eff}} = 5$ eV the degeneracy at M point remains protected. Without the SU(2) symmetry breaking and the SO-MO polarization introduced by SOC, as mentioned in the main text, the quadratic MO band touching at M point does not open a gap.

[1] G. Grüner, *Density Waves in Solids* (Westview Press, Boulder, CO, 2000).

[2] T. T. M. Palstra, A. A. Menovsky, J. van den Berg, A. J. Dirkmaat, P. H. Kes, G. J. Nieuwenhuys, and J. A. Mydosh, Phys. Rev. Lett. **55**, 2727 (1985).

[3] J. A. Mydosh and P. M. Oppeneer, Rev. Mod. Phys. **83**, 1301 (2011).

[4] A. Adam and H.-U. Schuster, Z. Anorg. Allg. Chem. **584**, 150 (1990).

[5] E. A. III, T. Ozawa, S. M. Kauzlarich, and R. R. Singh, J. Solid State Chem. **134**, 423 (1997).

[6] T. C. Ozawa, R. Pantoja, E. A. Axtell III, S. M. Kauzlarich, J. E. Greedan, M. Bieringer, and J. W. Richardson Jr., J. Solid State Chem. **153**, 275 (2000).

[7] R. H. Liu, D. Tan, Y. A. Song, Q. J. Li, Y. J. Yan, J. J. Ying, Y. L. Xie, X. F. Wang, and X. H. Chen, Phys. Rev. B **80**, 144516 (2009).

[8] Y. Huang, H. P. Wang, W. D. Wang, Y. G. Shi, and N. L. Wang, Phys. Rev. B **87**, 100507 (2013).

[9] S. Y. Tan, J. Jiang, Z. R. Ye, X. H. Niu, Y. Song, C. L. Zhang, P. C. Dai, B. P. Xie, X. C. Lai, and D. L. Feng, Sci. Rep. **5**, 9515 (2015).

[10] Y. G. Shi, H. P. Wang, X. Zhang, W. D. Wang, Y. Huang, and N. L. Wang, Phys. Rev. B **88**, 144513 (2013).

[11] W. E. Pickett, Phys. Rev. B **58**, 4335 (1998).

[12] D. J. Singh, New J. Phys. **14**, 123003 (2012).

[13] X.-W. Yan and Z.-Y. Lu, J. Phys.: Condens. Matter **25**, 365501 (2013).

[14] G. Fan, X. Zhang, Y. Shi, and J. Luo, Sci. China Phys. Mech. Astron. **56**, 2399 (2013).

[15] T. C. Ozawa and S. M. Kauzlarich, J. Cryst. Growth **265**, 571 (2004).

[16] In this work we employed two *ab initio* density functional theory codes: OPENMX [33,24] and Vienna *ab initio* simulation package [35,36]. Note that we did not incorporate magnetism in our calculations. Detailed parameter sets adopted in both of the calculations are in Appendix A.

[17] See Appendices A and B for computational detail and further information on electronic structures.

[18] Since $|d_{e_g}\rangle_{1,2} = \mp a|d_{x^2-y^2}\rangle_{1,2} - b|d_{3z^2-r^2}\rangle_{1,2}$, the eigenvalues $L_z^{\pm}$ are given as $\pm 2a^2/(a^2+b^2)$. Our result gives roughly $a{:}b = 3{:}1$, which yields $L_z^{\pm} \approx \pm\sqrt{3}$.

[19] G.-Q. Liu, V. N. Antonov, O. Jepsen, and O. K. Andersen, Phys. Rev. Lett. **101**, 026408 (2008).

[20] A. J. Millis, P. B. Littlewood, and B. I. Shraiman, Phys. Rev. Lett. **74**, 5144 (1995).

[21] T. Mizokawa and A. Fujimori, Phys. Rev. B **54**, 5368 (1996).

[22] T. Mizokawa, D. I. Khomskii, and G. A. Sawatzky, Phys. Rev. B **60**, 7309 (1999).

[23] E. Pavarini, S. Biermann, A. Poteryaev, A. I. Lichtenstein, A. Georges, and O. K. Andersen, Phys. Rev. Lett. **92**, 176403 (2004).

[24] G. Khaliullin, Prog. Theor. Phys. Supp. **160**, 155 (2005).

[25] P. G. Radaelli, New J. Phys. **7**, 53 (2005).

[26] G. Jackeli and N. B. Perkins, Phys. Rev. B **65**, 212402 (2002).

[27] G. van der Laan and B. T. Thole, Phys. Rev. Lett. **60**, 1977 (1988).

[28] B. Kim, H. Ohsumi, T. Komesu, S. Sakai, T. Morita, H. Takagi, and T. Arima, Science **323**, 1329 (2009).

[29] J. W. Kim, Y. Choi, J. Kim, J. F. Mitchell, G. Jackeli, M. Daghofer, J. van den Brink, G. Khaliullin, and B. J. Kim, Phys. Rev. Lett. **109**, 037204 (2012).

[30] T. Maitra and R. Valentí, Phys. Rev. Lett. **99**, 126401 (2007).

[31] H.-S. Jin, K.-H. Ahn, M.-C. Jung, and K.-W. Lee, Phys. Rev. B **90**, 205124 (2014).

[32] Y.-J. Song, K.-W. Lee, and W. E. Pickett, Phys. Rev. B **92**, 125109 (2015).

[33] T. Ozaki, Phys. Rev. B **67**, 155108 (2003).

[34] http://www.openmx-square.org.
[35] G. Kresse and J. Hafner, Phys. Rev. B **47**, 558 (1993).
[36] G. Kresse and J. Furthmüller, Phys. Rev. B **54**, 11169 (1996).
[37] D. M. Ceperley and B. J. Alder, Phys. Rev. Lett. **45**, 566 (1980).
[38] J. P. Perdew and A. Zunger, Phys. Rev. B **23**, 5048 (1981).
[39] S. L. Dudarev, G. A. Botton, S. Y. Savrasov, C. J. Humphreys, and A. P. Sutton, Phys. Rev. B **57**, 1505 (1998).
[40] M. J. Han, T. Ozaki, and J. Yu, Phys. Rev. B **73**, 045110 (2006).
[41] J. P. Perdew, A. Ruzsinszky, G. I. Csonka, O. A. Vydrov, G. E. Scuseria, L. A. Constantin, X. Zhou, and K. Burke, Phys. Rev. Lett. **100**, 136406 (2008).